UNIVERSITAT DE BARCELONA

Master in Quantum Science and Technology

Master Thesis

Quantum digital simulation of the Fermi-Hubbard model under a uniform electric field

Author: Joan Triadú i Galí

Co-Supervisors: Axel Pérez-Obiol
Artur Garcia Saéz

Barcelona Supercomputing Center
Centro Nacional de Supercomputación

Quantum digital simulation of the Fermi-Hubbard model under a uniform electric field

Joan Triadú i Galí

Supervised by: Axel Pérez-Obiol Castañeda & Artur Garcia Sáez

Barcelona Suercomputing Centre, Plaça Eusebi Güell, 08034 Barcelona

July 2023

In this study, we investigate the behaviour of the Fermi-Hubbard model when subjected to a uniform electric field, employing a digital quantum computing approach. Our research focuses on lattices with varying geometries, fillings, and interaction strengths between electrons. Initially, we develop an efficient adiabatic algorithm on a quantum circuit to prepare interacting ground states in the absence of electromagnetic fields. Afterwards, electric fields of different intensities are applied, and we employ the same quantum circuit to solve the time-dependent Schrödinger equation, enabling us to explore the system's response. Furthermore, we simulate a quench to gain further insights into the behaviour of the system. Finally, we implement a measurement protocol to obtain the expected value of the current at different times during the system's evolution. Our findings demonstrate that the response of the Fermi-Hubbard model is strongly influenced by the magnitude and duration of the applied electric field, as well as the electron-electron interaction. This work establishes a fundamental framework for studying the dynamics of strongly correlated electrons using digital quantum computers.

Keywords: Quantum computing, Fermi-Hubbard model, TFM

Acknowledgements

I want to acknowledge all the members of the BSC-Quantic research group for making me feel part of the group since day one. Also, I want to add a special mention to Axel. I am grateful for his time, his kindness, his guidance throughout the project, and for all the passionate discussions that we had about particles moving throughout a ring. Finally, I want to thank Alice for her priceless and unconditional support.

Joan Triadú i Galí: joan.triadu@bsc.es

Contents

1 Introduction

In the last decade, digital quantum computers have emerged as a new platform to simulate physical systems. Unlike classical computers, which face exponential computational challenges when simulating quantum many-body systems, quantum computers offer the potential to be efficient. The development of the first generation of noisy intermediate-scale quantum (NISQ) devices has played a crucial role in advancing this field. Although NISQ devices still have limitations, such as restricted qubit counts, limited gate fidelity, and shallow circuit depths, ongoing research aims to explore their potential for achieving a "quantum advantage" by outperforming classical computers in solving specific problems [DBK+22][GAN14][MLA+22].

In the field of digital quantum simulation, the majority of studies have focused on time-independent systems, where the behaviour of quantum states is examined under a fixed Hamiltonian. Various algorithms have been devised and tested to simulate quantum many-body systems of very different nature, such as molecules [DXP+10], crystals [POPSSR+22] and atomic nuclei [PORM+23]. These works study the ground state properties as the energy, the chemical potential or the charge density, often using second-quantization Hamiltonians, and mostly by variational approaches [SBG+22][CCBP+22]. This Master's thesis takes a less common approach by delving into the realm of dynamics, exploring the time evolution of quantum systems governed by a time-dependent Hamiltonian. Specifically, the investigation centers around the Fermi-Hubbard model.

The Fermi-Hubbard Hamiltonian consists of two main terms: the kinetic hopping term, which accounts for the movement of particles between neighbouring lattice sites, and the on-site interaction term, which represents the repulsion between particles occupying the same site. The model is considered a cornerstone in condensed matter physics and has been extensively studied due to its simplicity in describing interacting particles on a lattice.

The simulation of the dynamics of the Hubbard model has the potential to provide an in-depth quantitative analysis of physical characteristics beyond the phase diagram, revealing the underlying physics of the strongly correlated phases in the model. Few works have studied the response of the Fermi-Hubbard model under constant electric fields. In [Zhe22], a 1D non-interacting Fermi-Hubbard model is considered, and the period of the current oscillations that the system displays when subjected to the electric field is analytically derived. Quenches were studied by [M10] where persistent current oscillations of different characters were found depending on the correlation of the particles. Yet, studies of the application of electric fields to the Fermi-Hubbard model remain relatively scarce in the existing literature, in part due to the exponential computational cost to simulate large systems. Furthermore, there have been no digital quantum computing approaches in this context, indicating a significant gap in knowledge.

In this study, we aim to fill this gap by examining the response of two specific systems, namely a 1×8 ring and a 4×2 stacked ring, to a uniform electric field at zero temperature ($T = 0K$). We investigate three distinct scenarios: non-interacting, weak, and strong Coulombian coupling. In the 1×8 ring, we focus on two different odd-odd fillings, namely $n_\uparrow = 1$, $n_\downarrow = 1$ and $n_\uparrow = 3$, $n_\downarrow = 3$. For the 4×2 stacked ring, our analysis focuses on the case with filling $n_\uparrow = 1$, $n_\downarrow = 1$.

To start the simulation we prepare the time-independent ground state of the Fermi-Hubbard model using a quantum adiabatic algorithm, as in [POPSSR+22]. Then, we apply two different electric fields coming from a linearly increasing magnetic flux to each system. The first field is relatively strong, while the second field is weaker. The application of different fields allows us to compare the dynamics of the systems under varying field

strengths. We also study a case in which we simulate a sudden turn-off of the electric field, ie. a quench, to try to infer the properties of the instantaneous wave functions of the systems. By analyzing these responses, we aim to gain deeper insights into the influence of electric fields on the Fermi-Hubbard model to contribute to the understanding of the dynamics of strongly correlated fermions.

Although the quantum circuits have been run on a statevector simulator, we have also prepared the measurement algorithm for the 1×8 ring, so the protocol could be run on a real-life quantum computer.

From now on, the work is organized as follows. In the next section, we introduce the Fermi-Hubbard model and its basic properties with and without an electric field. Next, in section 3, we explain the main steps of the devised quantum algorithm to simulate the Fermi-Hubbard model under an electric field, including the measurement protocol to compute the charge current. We show our results in section 4 and discuss them in section 5.

2 The Fermi-Hubbard Model

Band theory has been a highly successful framework for understanding electron behaviour in solids. However, its limitations become apparent in cases such as Mott insulators, where an odd number of valence electrons per elementary cell results in an insulating phase, contrary to band theory predictions. In the 1960s, the Hubbard model emerged as a formalism beyond band theory, offering a simplified yet insightful representation of interacting particles in a lattice structure. In Appendix A there is the derivation of the Fermi-Hubbard model from first quantization. It has many variations but the standard form of the model reads,

$$\hat{H}_0 = \underbrace{-J \sum_{\langle i,j\rangle,\sigma} \left(\hat{c}^\dagger_{i\sigma}\hat{c}_{j\sigma} + \hat{c}^\dagger_{j\sigma}\hat{c}_{i\sigma}\right)}_{H_{hopp}} + U \sum_{i}^{L} \hat{n}_{i\uparrow}\hat{n}_{i\downarrow} \tag{1}$$

where $\hat{c}^\dagger_{i\sigma}$ and $\hat{c}_{i\sigma}$ are the operators that create and annihilate an electron of spin $\sigma = \{\uparrow, \downarrow\}$ at the i-site respectively, $\hat{n}_{i\sigma} = \hat{c}^\dagger_{i\sigma}\hat{c}_{i\sigma}$ is the number operator, J is the hopping coefficient, U the on-site interaction strength and L the number of sites. The hopping coefficient is usually written as t, but we use another notation to avoid confusion with time. Also, we fix $J = 1$ since the relevant magnitude is U/J.

As presented in eq.(1), the Hubbard Hamiltonian starts from the tight-binding Hamiltonian (H_{hopp}) and incorporates an on-site two-body interaction, becoming one of the simplest models of correlated fermions. The first term contributes to delocalise fermions and the second forces localisation, reason why the Hubbard Hamiltonian is often seen as an interplay between the hopping kinetic term and the Coulombian interaction. Despite its simplicity, there is still much to discover about the characteristics of the model, which is why apart from Mott insulators, the Hubbard model has been used to study high-temperature superconductivity, quantum magnetism, and anomalous quantum phases.

It is important to note that although the two terms of the Hamiltonian can be diagonalized separately, they do not commute, ie. they can not be diagonalized simultaneously. This makes the Hamiltonian unsolvable in most cases, although at particular dimensionalities and parameter values is exactly solvable. The most general solution is in the 1D case, which was solved 5 years after the publication of the John Hubbard paper [fho63] by the Bethe-Ansatz [LW68]. The diagonalization of each term is done in Appendix B.

2.1 Electromagnetic coupling

In this work, we will not be using the standard form of the Fermi-Hubbard model since we are interested in studying the effects of an electromagnetic field, so we need to couple the field into the Hamiltonian. This step is done by the so-called Peierls substitution which adds a phase to the hopping term. Moreover, we add two extra terms in the Hamiltonian: the chemical potential (μ) and the coupling of the spins to an external magnetic field (b). We only use these terms to custom the number and spin of the particles when preparing the ground state with our quantum algorithm, but we are not interested in their physical meaning. After these modifications, the Hamiltonian reads,

$$\hat{H} = -J \sum_{\langle i,j\rangle,\sigma} \left(e^{i\phi} \hat{c}^\dagger_{i\sigma} \hat{c}_{j\sigma} + e^{-i\phi} \hat{c}^\dagger_{j\sigma} \hat{c}_{i\sigma} \right) + U \sum_i \hat{n}_{i\uparrow} \hat{n}_{i\downarrow} + \underbrace{\mu \sum_{i,\sigma} \hat{n}_{i,\sigma} - b \sum_i (\hat{n}_{i,\uparrow} - \hat{n}_{i,\downarrow})}_{H_{\mu b}} \quad (2)$$

where

$$\phi = \frac{e}{c\hbar} \int_{\mathbf{r}_i}^{\mathbf{r}_j} \mathbf{A} \cdot \mathbf{dl} \quad (3)$$

is the Peierls phase with $\mathbf{A}$ being the electromagnetic potential. As it is evident from the equation above, the Peierls phase critically depends on the geometry of the system studied. We consider a 1D chain with periodic boundary conditions, ie. a ring, Figure 1a). In these conditions, the Hamiltonian is,

$$\hat{H}_{1D} = \underbrace{-J \sum_{i,\sigma}^{L} \left(e^{i\phi} \hat{c}^\dagger_{i+1\sigma} \hat{c}_{i\sigma} + e^{-i\phi} \hat{c}^\dagger_{i\sigma} \hat{c}_{i+1\sigma} \right)}_{H_{hopp'}} + \underbrace{U \sum_{i}^{L} \hat{n}_{i\uparrow} \hat{n}_{i\downarrow}}_{H_C} + H_{\mu b} \quad (4)$$

where the periodic boundary conditions establish $\hat{c}_{L+1\sigma} = \hat{c}_{1\sigma}$. The Peierls phase also depends on the direction of the fields that one aims to study. We consider a uniform magnetic field threading the ring and a uniform electric field parallel to the ring. In these cases, the Peierls phase in natural units ($c = 1$) reads respectively,

$$\phi_{\mathbf{B}} = \frac{2\pi\Phi}{L\Phi_0} \quad (5)$$

$$\phi_{\mathbf{E}} = \frac{2\pi a}{\Phi_0} E_0 \cdot t \quad (6)$$

where Φ is the magnetic flux, Φ_0 the flux quantum, $a = \frac{2\pi R}{L}$ is the lattice parameter and E_0 the intensity of the electric field, that is created by a linearly increasing the magnetic flux threading the ring. Note that the coupling of an electric field needs a time-dependent Hamiltonian, while the magnetic field does not. The computation of the Peierls phase for each scenario is detailed in Appendix C.

We also consider the case of two rings stacked, one above the other, Figure 1b). The Peierls phase calculation is easily extended in this geometry and it turns out that is equal to the one-ring case for the hopping within the same leg and it vanishes for the inter-leg hopping. The Hamiltonian reads,

$$\hat{H}_{2D} = -J \sum_{i,\sigma,l}^{L} \left(e^{i\phi} \hat{c}^\dagger_{(i+1)\sigma l} \hat{c}_{i\sigma l} + h.c. \right) - J_\perp \sum_{i,\sigma}^{L} \left(\hat{c}^\dagger_{i\sigma u} \hat{c}_{i\sigma d} + h.c. \right) + U \sum_{i,l}^{L} \hat{n}_{il\uparrow} \hat{n}_{il\downarrow} + H_{\mu b} \quad (7)$$

where the index $l = \{u, d\}$ runs on the top (u) and bottom (d) legs and $J_\perp$ is the inter-leg hopping coefficient. Here, L denotes the number of orbitals in one leg. The periodic boundary conditions establish $\hat{c}_{L+1\sigma l} = \hat{c}_{1\sigma l}$. We have fixed $J = J_\perp = 1$.

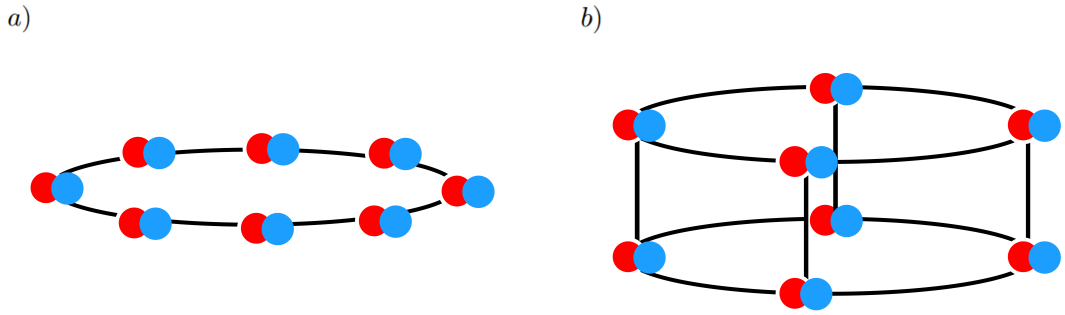

Figure 1: a) 1D chain with periodic boundary conditions with $L = 8$. b) 4×2 Stacked ring. Each pair of circles represent an orbital where two electrons fit, and the black lines show the connectivity of the orbitals.

2.2 Equilibrium properties of the Fermi-Hubbard model

Before studying the dynamics of the Fermi-Hubbard model in terms of the electric field, it is convenient to see how the magnetic flux governs the ground state properties at equilibrium. If we Fourier-transform the single ring Hamiltonian in eq.(4) with $U = 0$ and $\phi = \phi_{\mathbf{B}}$, the final Hamiltonian is diagonal and has eigenvalues:

$$E(\Phi) = -2J \sum_{k,\sigma} \cos\left(\frac{2\pi}{L}(k - \frac{\Phi}{\Phi_0})\right) \tag{8}$$

The equation reveals that the ground state energy has the periodicity of the flux quantum since the lowest energy level intersects with the first excited state at each $\Phi = \Phi_0$. The appearance of this Φ_0 periodicity is due to the Aharonov-Bohm effect, detailed in Appendix D. With a quick calculation, one can realise that depending on the parity of the number of particles, the intersection happens at integers or half integers of the flux quantum. Considering spinless fermions, if the number of particles is even, the intersection between the ground and the excited state is at integers of flux quantum. This translates to a paramagnetic behaviour since the energy decreases when flux is applied. Alternatively, if the number of particles is odd, the behaviour is diamagnetic: the intersection is at half flux quantum so the energy of the ground state increases with the application of flux.

In Figure 2 there is represented the case of electrons ($SU(2)$ fermions) where we have to consider separately the spin-up and spin-down particles as if there were two rings. Exactly as in the spinless case, when the number of particles is even-even we have paramagnetic behaviour, and if we have an odd-odd occupation, we return to the diamagnetic case. Interestingly, when the combination is odd-even or even-odd, the energy shows paramagnetic behaviour but with the period halved [ES98].

Remarkably, the energy periodicity creates an eternal and non-dissipative current throughout the ring, known as the persistent current. The charge current at $T = 0K$ and in the rotating reference frame is defined as,

$$I(\Phi) = -\frac{\partial E_0}{\partial \Phi} \tag{9}$$

where E_0 denotes the lowest energy of eq.(8). We can see that deriving eq.(8) and plotting the current where each eigenstate is the ground state, a persistent current appears, see Figure 2. The characteristic saw-tooth shape reflects the periodic behaviour of the spectrum.

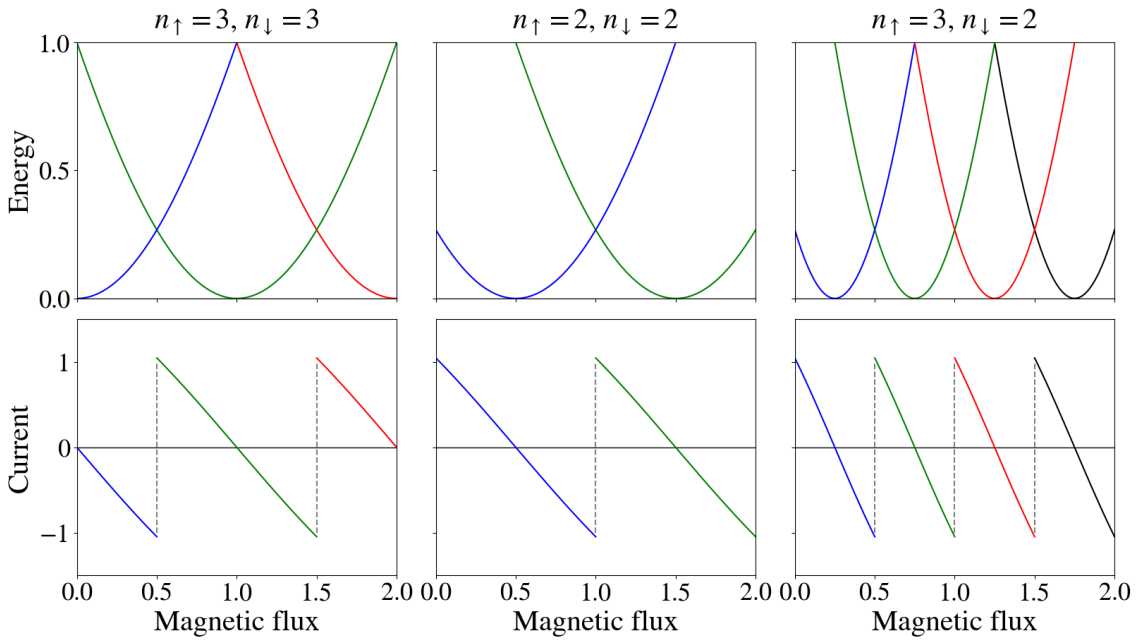

Figure 2: Spectrum and persistent current of a 1×6 non-interacting Fermi-Hubbard ring. Columns show different fillings.

The implications of the Aharanov-Bohm effect on the Fermi-Hubbard model are sensitive to a vast variety of parameters, an example of which is the correlation between electrons. When adding repulsive interaction between electrons the persistent current remains, but the amplitude and the period of the oscillation can change with respect to the non-interacting case. Even the characteristic saw-tooth shape can disappear. There is not a general solution for the behaviour of the current in terms of the electronic correlations, but it has been extensively studied throughout the last decades by classical numerical methods [CRG89][SM16][MCK04], and recently from a digital quantum computing variational approach [CCBP+22]. That is why we want to go a step further and explore the non-equilibrium regime that appears when applying a time-dependent flux, ie. an electric field.

We want to mention that precisely because the equilibrium regime is governed by the flux, many prefer to speak in terms of time-dependent magnetic flux instead of electric field, but we find that the electric field is an intuitive magnitude which can be helpful to understand the physics of the Hubbard model.

2.3 Electric field in the Fermi-Hubbard model

The study of non-equilibrium properties in strongly correlated electron systems is a subject of great interest in condensed matter physics. The influence of electron-electron interactions on a system's response to external fields can result in complex transport phenomena. Particularly, the Hubbard model has provided valuable insights on this topic but there is not a full understanding of the model's transport properties, which is why there is still ongoing research in this field.

Recently, Zheng proved analytically that the charge current response under an electric field displays persistent oscillations with a periodicity of

$$\tau = \frac{\Phi_0}{a \cdot E_0} \tag{10}$$

defying conventional expectations observed in normal metal conductors [Zhe22]. Interestingly, oscillating current states exhibit neither decay into a steady state nor constant increase over time, even in the presence of strong electronic correlation interactions. However, his works are focused only on the non-interacting and the infinite repulsion cases [Zhe21]. Other works have studied the role of on-site electron correlations in shaping the system's response to electric fields. For example, it has been shown through a numerical simulation that the charge current results in either damped or over-damped Bloch oscillations depending on the magnitude of the on-site correlation, in an infinite-dimensional Fermi-Hubbard model with finite temperature [EW11]. There is not much further literature about the application of the electric field to the Fermi-Hubbard model and as far as we know, there has not been any digital quantum computing approach, so there is still room to explore.

In this work, we assess the response of a 1×8 ring and a 4×2 stacked ring to a uniform electric field, in the framework of the Fermi-Hubbard model at $T = 0K$. We study the non-interacting, weak, and strong Coulombian coupling cases ($U = 0, 1, 5$ respectively). In the 1×8 ring we see two different odd-odd fillings ($n_\uparrow = 1$, $n_\downarrow = 1$ and $n_\uparrow = 3$, $n_\downarrow = 3$) and in the 4×2 we focus on the $n_\uparrow = 1$, $n_\downarrow = 1$ case. To see how the response changes with the intensity of the field, two different electric fields are applied to each system, a strong one and a weaker one, starting from $\Phi = 0$:

$$\text{Weak field} \longrightarrow E_w \approx 10^{-2} \cdot \frac{\Phi_0}{t} = \text{constant} \tag{11}$$

$$\text{Strong field} \longrightarrow E_s \approx 10^{-1} \cdot \frac{\Phi_0}{t} = \text{constant} \tag{12}$$

where t is time in natural units.

With this procedure, our first goal is to observe the oscillations of the charge current that have the period as in eq.(10). Notice that this periodicity is the same that in eq.(8), which suggests that when applying an electric field (caused by a linearly increasing magnetic flux), the system follows the blue parabolas in Figure 2 all the way up (and down), instead of changing the state every $\Phi_0/2$, as it happens in equilibrium. For clarity, we show the explicit calculations. The period in eq.(8) in terms of the flux is:

$$\Phi = \Phi_0 \cdot L$$

If we have a linearly increasing flux in time,

$$\Phi(t) = E_0 \cdot 2\pi R \cdot t$$

the temporal period becomes

$$T = \frac{L\Phi_0}{2\pi R \cdot E_0} = \frac{\Phi_0}{a \cdot E_0}$$

We want to study if this periodicity is the same when electrons are correlated, in other words, we want to assess whether the Coulombian interactions break the smooth and non-decaying oscillations described by [Zhe22]. Secondly, we want to see if the amplitude of the oscillations depends on the electric field. We will do the analysis for all the fillings, interaction regimes and geometries, explained above.

Afterwards, we also study the reaction of each system when performing a quench, that is, suddenly turning the electric field off. We use electric fields of the same magnitude as

the previous case, and perform the quench at time $t = \frac{\Phi_0}{E}$, or equivalently, when the flux that threads the ring gets up to a flux quantum. By doing this, we aim to infer properties of the dynamical evolution of the system without having to resort to the time-independent spectrum, which is exponentially costly to obtain with growing L.

3 Quantum algorithm

We study our physical systems in a digital quantum computing framework, so we develop an algorithm using quantum circuits to prepare, evolve and measure our qubits. Throughout the algorithm design, we assumed local interactions (only adjacent qubits can interact) and linear connectivity (qubits form a non-periodic chain). The circuits have been programmed in *Qibo* [ERCBP+22] and run in its backend simulator with an ordinary laptop.

3.1 Mapping

The first step to perform the digital quantum simulation is to map the sites of the Hamiltonian to qubits. It is important to bear in mind that in each site fit two electrons, so we need twice as many qubits as sites. In the ring, the correspondence between sites and qubits is really simple, even qubits represent spin-up orbitals and odd qubits the spin-down ones. In the 2D case, the qubits trace a snakelike pattern along the chain, therefore, spin-down orbitals are represented with odd qubits in the top row and even qubits in the bottom. With the spin-up orbitals happens analogously, see Figure 3.

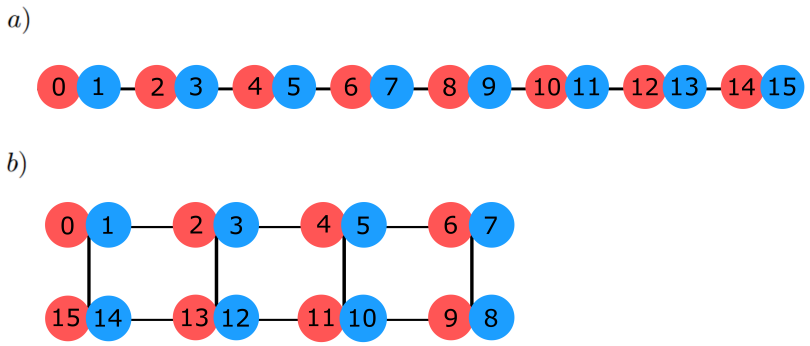

Figure 3: Correspondence between qubits and sites for a) the single ring b) the stacked ring. Red circles represent spin-up orbitals and blue ones spin-down.

Then, with the Jordan-Wigner transformation, very common in condensed matter simulation [POPSSR+22][SBG+22], we map the fermionic operators into Pauli-strings:

$$\hat{c}_j^\dagger = \prod_{k=0}^{j-1} \sigma_k^{(z)} \frac{1}{2}(\sigma_j^{(x)} + i\sigma_j^{(y)}) \tag{13}$$

$$\hat{c}_j = \prod_{k=0}^{j-1} \sigma_k^{(z)} \frac{1}{2}(\sigma_j^{(x)} - i\sigma_j^{(y)}) \tag{14}$$

where the string $\prod_{k=0}^{j-1} \sigma_k^{(z)}$ is used to preserve the anticommutation relations of fermionic operators.

3.2 Ground state preparation

In this section, we develop a method to obtain the stationary ground state of Fermi-Hubbard Hamiltonians as in eq.(4, 7). We split the preparation into two parts. First, we prepare the state with $U = 0$. Then, we use this state to prepare the ground state of the full Fermi-Hubbard model with $U > 0$ by adiabatically switching on U.

3.2.1 Non-interacting ground state, $U = 0$

To prepare the non-interacting ground state of the Fermi-Hubbard model with a quantum circuit we use the procedure developed in [JSK+18], which allows us to prepare the ground state of any fermionic quadratic Hamiltonian of the form,

$$H = \sum_{j,k=1}^{N} M_{jk}\hat{c}_j^\dagger \hat{c}_k + \frac{1}{2}\sum_{j,k=1}^{N}\left(\Delta_{jk}\hat{c}_j^\dagger \hat{c}_k^\dagger + h.c.\right) \tag{15}$$

where $M = M^\dagger$ and $\Delta = -\Delta^T$ are complex matrices. The protocol consists first in applying X gates to certain qubits and then applying a series of Givens rotations $G(\theta, \varphi)$,

$$G(\theta,\varphi) = \begin{pmatrix} \cos\theta & -\sin\theta \\ \sin\theta & \cos\theta \end{pmatrix}\begin{pmatrix} 1 & 0 \\ 0 & e^{i\varphi} \end{pmatrix} = \begin{pmatrix} \cos\theta & -e^{i\varphi}\sin\theta \\ \sin\theta & e^{i\varphi}\cos\theta \end{pmatrix} \tag{16}$$

encoded in the Jordan-Wigner transformation. This combination of gates diagonalizes the non-interacting Hamiltonian, so we obtain the exact ground state. Givens rotations are not supported in *Qibo* but they can be constructed with a *GeneralizedfSim* gate. (Note that Givens rotations are often written with a factor 2 dividing the θ [SBG+22], so one must take this into account when looking at different sources). This ground state preparation algorithm needs $O(N^2)$ gates and $O(N)$ circuit depth, where N is the number of qubits, so it is reasonably efficient.

Our Hamiltonians in eq.(4,7) are quadratic for $U = 0$, so we use this protocol to find the non-interacting ground state with the implementation that the authors did in *Python* as part of the *Openfermion* project. The only limitation existing in this procedure is that one can not fix the number of particles, that is why we have introduced a chemical potential and a spin coupling in our Hamiltonians. We must say though, that with these extra terms in the Hamiltonian we did not have unlimited freedom to choose the number of particles and their spins because many combinations are never the ground state of the L-sites Hamiltonian, so we can not prepare those states. Further work could be done to overcome this limitation.

3.2.2 Interacting ground state, $U > 0$

To prepare an interacting ground state we take advantage of the Adiabatic theorem. The theorem states that a physical system will stay in its instantaneous eigenstate if it is subjected to a slow and gradual perturbation, and there exists a gap between its instantaneous eigenstate and the rest of the Hamiltonian's spectrum (throughout the perturbation process) [BF28][Kat50]. This occurs because the system has sufficient time to adapt gradually to the perturbation without transitioning to other eigenstates. The evolution time must be at least $O(\Delta E^2)$, where ΔE is the gap between the ground and the first-excited states. This means that if we start with a non-interacting ground state and we introduce the interaction term slowly enough, we arrive at the interacting ground state at the end of the evolution. In our results, an energy gap between the ground state and the first excited

state is assumed because the existence of a gap is not known a priori for these systems. The following explanations detailing how we use the Adiabatic theorem to obtain a time-independent ground state are focused on the single ring Hamiltonian in eq.(4) but the procedure it's easy to extend to the Hamiltonian of two stacked rings as in eq.(7).

As we mentioned, our initial state is the ground state of the time-independent Hamiltonian for $U = 0$, ie. the ground state of $H_{hopp'}$. Let's call this state $|\psi(0)\rangle$, and remind that it can be exactly obtained with the protocol of the previous section. Now, let's consider the following time-dependent Hamiltonian,

$$\hat{H}_{adiab}(s) = (1-s)\cdot H_{hopp'} + s\cdot \hat{H}_{1D} = H_{hopp'} + s\cdot H_C + H_{\mu b}, \qquad s = \frac{t}{T} \in [0,1] \quad (17)$$

where t is the time and T is the total evolution time. If we solve the time-dependent Schrödinger equation, we get, formally,

$$|\psi(T)\rangle = \hat{\mathcal{T}} e^{-i\int_0^T \hat{H}_{adiab}(t)dt} |\psi(0)\rangle \quad (18)$$

where $\hat{\mathcal{T}}$ is the time ordering operator. To perform the simulation we have to transform the integral into a product,

$$|\psi(T)\rangle \approx \prod_{j=0}^{N} e^{-i\hat{H}_{adiab}(j\delta t)\delta t} |\psi(0)\rangle \quad (19)$$

where $\delta t = T/N$ and N the total number of time-steps. Our goal is to simulate this evolution on a quantum device but real-life quantum computers can only perform gates involving one or two qubits, so it is necessary to decompose $e^{-iH(\hat{j}\delta t)\delta t}$ gate into simpler operations. Fortunately, we can use the Trotter-Suzuki formula

$$e^{-i\delta t\hat{H}_{adiab}(j\delta t)} = e^{-i\delta t\frac{j\cdot\delta t}{T}\cdot H_C} e^{-i\delta t H_{hopp'}} + O([H_{hopp'}, H_c], \delta t^2) \quad (20)$$

that allows us to separate the two main terms of the Hamiltonian with an error proportional to δt^2. $H_{hopp'}$ and H_C are themselves a sum of operators, so we apply this formula recursively to separate each sum until we only have two-body matrices (which can be applied in quantum computers as 2-qubit gates). The key part of the adiabatic algorithm is to understand that T and δt are two independent parameters which must be chosen carefully because the performance of the algorithm can vary depending on their values. This happens because each of these parameters represents a source of error: δt is related to the error of Trotterization, and T to the error of adiabatic approximation.

Note that in the previous step we have removed the $H_{\mu b}$ term since the evolving Hamiltonian of eq.(17) conserves the number of particles ($[\hat{H}, \hat{n}] = 0$). If all the basis elements of $|\psi(0)\rangle$ have the same number of particles and spins-up (and spin-down), this term would only add a global phase in the time evolution. As the ground states we work with fulfil the latter condition, we can remove this term from the evolution Hamiltonian.

Taking it all into account the time evolution reads:

$$|\psi(T)\rangle \approx \prod_{j=0}^{N}\prod_{i}^{L} e^{-i\delta t\frac{j\delta t}{T}U\hat{n}_{i\uparrow}\hat{n}_{i\downarrow}} \prod_{i\sigma}^{L} e^{i\delta t J(e^{i\phi}\hat{a}^\dagger_{i+1\sigma}\hat{a}_{i\sigma} + e^{-i\phi}\hat{a}^\dagger_{i\sigma}\hat{a}_{i+1\sigma})} |\psi(0)\rangle \quad (21)$$

This process of dividing the Hamiltonian into parts is known as Trotterization. It is important to note that all the terms in H_C commute with each other so they can be applied simultaneously and do not contribute to the Trotter error separately. Nevertheless,

the hopping terms that involve repeated indices do not commute, so they are a source of error.

In summary, with the evolution of (21) and picking the proper δt and T parameters, one can access the interacting ground state starting from a non-interacting one. Now, we will further detail which form take the Trotter steps of our simulations.

Description of a Trotter step

For clarity reasons, we explicit the form of the two-qubit matrices that are run in the circuit when using the Jordan-Wigner mapping. First, we develop the two-body interaction matrices and afterwards their exponential. The two-body Coulombian interaction with the adiabatic term s reads:

$$s \cdot h_C = s \cdot U \cdot \hat{n}_{i\uparrow}\hat{n}_{i\downarrow} = s \cdot U \begin{pmatrix} 0 & 0 & 0 & 0 \\ 0 & 0 & 0 & 0 \\ 0 & 0 & 0 & 0 \\ 0 & 0 & 0 & 1 \end{pmatrix} \tag{22}$$

If we compute the evolution operator, it takes the form of the $CU1$ gate supported in *Qibo*:

$$e^{-i\delta t \cdot s \cdot h_C} = \begin{pmatrix} 1 & 0 & 0 & 0 \\ 0 & 1 & 0 & 0 \\ 0 & 0 & 1 & 0 \\ 0 & 0 & 0 & e^{-i\delta t s U} \end{pmatrix} \tag{23}$$

The application of the hopping interaction is a bit trickier. Although we have reduced our Hamiltonian to two-body matrices, there are interactions between non-adjacent qubits in the hopping term. As we assumed linear connectivity we have to bring them together to interact. However, every time we switch two qubits we must ensure that the fermionic anticommutation is conserved. The FSWAP gate does exactly this

$$\text{FSWAP} = \begin{pmatrix} 1 & 0 & 0 & 0 \\ 0 & 0 & 1 & 0 \\ 0 & 1 & 0 & 0 \\ 0 & 0 & 0 & -1 \end{pmatrix} \tag{24}$$

Once the two qubits are put together using FSWAPS, the hopping operator reads,

$$h_h = -J(e^{i\phi}\hat{a}^\dagger_{i+1}\hat{a}_i + e^{-i\phi}\hat{a}^\dagger_i\hat{a}_{i+1}) = -J \begin{pmatrix} 0 & 0 & 0 & 0 \\ 0 & 0 & e^{-i\phi} & 0 \\ 0 & e^{i\phi} & 0 & 0 \\ 0 & 0 & 0 & 0 \end{pmatrix} \tag{25}$$

And the corresponding time evolution operator is

$$e^{-i\delta t h_h} = \begin{pmatrix} 1 & 0 & 0 & 0 \\ 0 & \cos(J\delta t) & ie^{-i\phi}\sin(J\delta t) & 0 \\ 0 & ie^{i\phi}\sin(J\delta t) & \cos(J\delta t) & 0 \\ 0 & 0 & 0 & 1 \end{pmatrix}$$

This gate is not supported in *Qibo* but it can be built with a GeneralizedfSim gate, as it happened with the Givens rotations. However, if we prepare a state with $\mathbf{B} = 0$ the Peierls phase vanishes ($\phi = 0$) and this interaction can be implemented with a fSim gate. It is relevant to mention that each quantum computer has native one and two-qubit gates

which do not have to be the ones we used. As we run our circuits in a Qibo simulator and not in a particular quantum computer, we did not do the work of decomposing the gates into native ones.

The steps to perform the hopping interaction are key to optimising the number of gates and the time duration of the circuit, precisely because we have to add FSWAP gates every time we want to simulate the interaction. However, it is not necessary to rearrange the initial configuration in each interaction, so by optimizing this process we can build a better circuit. That is why, creating a quantum circuit is non-trivial, because one wants to minimize the depth[1] and the number of gates while preserving all the physical laws underlying the simulation. Two quantum circuits have been created, one for each geometry. We will start discussing the corresponding to the 1×8 ring, represented in Figure 4.

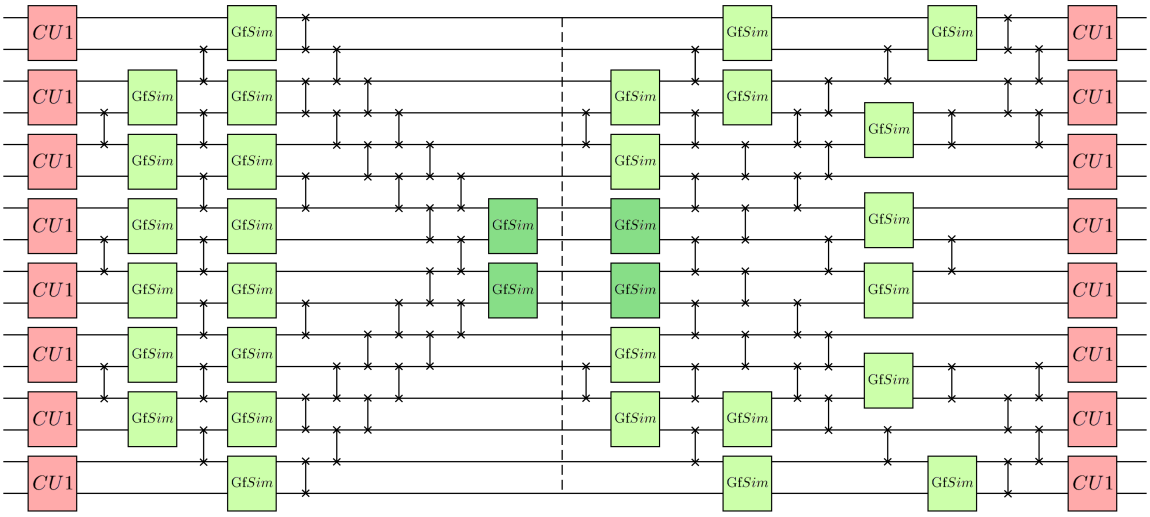

Figure 4: Two Trotter steps of the 1×8 ring circuit divided by a dashed line. Qubits are represented by horizontal black lines. The squares that overlap them are the corresponding two-qubit gates. Gates in darker green apply the periodic boundary condition hopping interaction. The lines connecting two qubits, with the crosses at their ends, represent the FSWAP gates. The horizontal axis is time running from left to right.

As discussed in the mapping section, we need 16 qubits to simulate the 1×8 ring. We first apply the on-site Coulombian interaction, which involves adjacent qubits in the computational basis and then we apply FSWAP gates to perform the hopping interaction. As it is clear in the figure, the periodic hopping interaction is the interaction that requires more depth and gates. Once we arrive at the dashed line, we have already applied a Trotter step but we have the qubits disarranged. We apply a second round of interactions while bringing them back to their initial positions instead of only rearranging them, to optimize the depth of the circuit.

This circuit has 59 gates and 12 layers of depth per Trotter step. Note that the second Trotter step could be symmetric with the dashed line, but if we do it like in the figure, the first gates after the dashed line can be applied in parallel to the last gates of the previous Trotter step, just before the dashed line. With this configuration, we subtract one unit of depth from the circuit. In general, if we follow the same circuit configuration given a

[1]The depth of the circuit is its number of layers, and it is not equal to the total number of gates since some gates can be performed in parallel.

number of qubits N, the number of gates per Trotter step is

$$\text{Number of gates} = \frac{9N}{2} - 13 = 9L - 13, \qquad \text{for } \frac{N}{2} \text{ even (or L even)} \tag{26}$$

$$\text{Number of gates} = \frac{9N}{2} - 9 = 9(L-1), \qquad \text{for } \frac{N}{2} \text{ odd (or L odd)} \tag{27}$$

Regarding the depth of the circuit per Trotter step:

$$\text{Circuit depth} = \frac{N+7}{2} = L + \frac{7}{2}, \qquad \text{for } \frac{N}{2} \text{ even (or L even)} \tag{28}$$

$$\text{Circuit depth} = \frac{N+9}{2} = L + \frac{9}{2}, \qquad \text{for } \frac{N}{2} \text{ odd (or L odd)} \tag{29}$$

where the semi-integer appears due to saving one layer of depth every 2 Trotter steps, as we already mentioned. The extra gates and depth for the odd L case are due to the asymmetry of the circuit in those cases. However, in all cases, scaling of the circuit depth and scaling of the total number of gates is linear with the number of sites, so we can say that this circuit is efficient.

The circuit of the 4×2 stacked ring has a different shape because the mapping and the interactions are substantially different. A single Trotter step is displayed in Figure 5, but again, at the end of this circuit, the qubits are disarranged. We have to run this circuit an even number of times to have the final state in the same qubit ordering as the initial one. We also start with the on-site interaction and then apply the hopping terms. The fSim

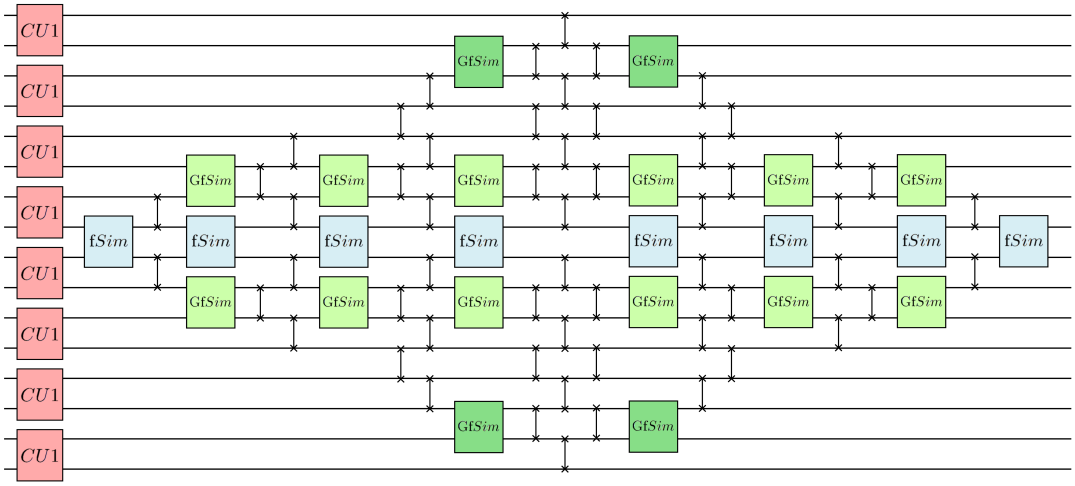

Figure 5: Single Trotter step of the 4×2 stacked-ring circuit. Qubits are represented by horizontal black lines. The squares that overlap them are the corresponding two-qubit gates. Gates in darker green apply the periodic boundary condition hopping interaction. Gates in blue apply the phase-less inter-leg hopping interaction. The lines connecting two qubits with the crosses at their ends represent the FSWAP gates. The horizontal axis is time, running from left to right.

gates (in blue) stand for the inter-leg hopping term, and we can use a different gate since this interaction does not carry any Peierls phase. This circuit has 88 gates and 22 circuit layers. If we follow the same structure but with a different number of qubits (or sites) the number of gates and the depth is

$$\text{Number of gates} = \frac{N}{4}(N+6) = 2L(2L+3) \tag{30}$$

$$\text{Circuit depth} = \frac{3N}{2} - 2 = 6L - 2 \tag{31}$$

where $L = \frac{N}{4}$ is the number of sites in a leg and N is the number of qubits.

3.3 Evolution

Once we know how to prepare the initial states, we are ready to apply the electric field. To do so, we have to solve (again) the time-dependent Schrödinger equation for the Hamiltonians,

$$\hat{H}_{1D} = -J \sum_{i,\sigma}^{L} \left(e^{i\phi_E} \hat{c}^\dagger_{i+1\sigma} \hat{c}_{i\sigma} + e^{-i\phi_E} \hat{c}^\dagger_{i\sigma} \hat{c}_{i+1\sigma} \right) + U \sum_{i}^{L} \hat{n}_{i\uparrow} \hat{n}_i \tag{32}$$

$$\hat{H}_{2D} = -J \sum_{i,\sigma,l}^{L} \left(e^{i\phi} \hat{c}^\dagger_{(i+1)\sigma l} \hat{c}_{i\sigma l} + h.c. \right) - J_\perp \sum_{i,\sigma}^{L} \left(\hat{c}^\dagger_{i\sigma u} \hat{c}_{i\sigma d} + h.c. \right) + U \sum_{i,l}^{L} \hat{n}_{il\uparrow} \hat{n}_{il\downarrow} \tag{33}$$

We solve the equation by discretizing and Trotterizing the Hamiltonians once again. For the 1D case,

$$|\psi(T)\rangle \approx \prod_{j=0}^{N} \prod_{i}^{L} e^{-i\delta t U \hat{n}_{i\uparrow} \hat{n}_{i\downarrow}} \prod_{i\sigma}^{L} e^{i\delta t J (e^{i\phi} \hat{a}^\dagger_{i+1\sigma} \hat{a}_{i\sigma} + e^{-i\phi} \hat{a}^\dagger_{i\sigma} \hat{a}_{i+1\sigma})} |\psi(0)\rangle \tag{34}$$

and for the stacked ring analogous. This time, our goal is to study the real time evolution of the system, and not to add adiabatically a time-indepdendent term. However, the solution is formally equivalent to the adiabatic case, so we can use the circuits described in the previous section to perform the time-evolution. As we can see in eq.(34), there isn't anymore a factor s in the Coulombian interaction term. This time the Peierls phase is

$$\phi_E = \frac{2\pi}{L} E_0 \cdot j \cdot \delta t$$

where we have taken $\Phi_0 = 1$ and $a = \frac{1}{L}$ for simplicity. Regarding the quench case, when we turn off the electric field at $E_0 \cdot j \cdot \delta t = 1$, we maintain the Peierls phase to its maximal value. In other words, to turn off the electric field we stop increasing the flux, and its final value is $\Phi = \Phi_0$. Then, the Peierls phase after the quench is

$$\phi = \frac{2\pi}{L}$$

3.4 Measurement

In this work, we have run our algorithms in a statevector simulator so that to measure any physical observable we could just apply the corresponding matrices to the final state and compute the expected value. However, for the 1×8 ring we also simulated the measurement of the observables as if we ran the circuits on a real quantum computer.

Measuring observables in a quantum computer is not straightforward, since one can not access the full wave function. One can only measure the qubits and obtain an element of the computational basis, which corresponds to the collapsed state. As it is a quantum system, the outcome of the measurement is probably not the only state that conformed the wave function, so one must repeat the entire algorithm and the measurement to collect statistics of the outcome. If the observable in question is diagonal with the computational basis, which means that its eigenvectors are the elements of the computational basis, these are the only steps to follow. One can compute the expected value of this operator with

the frequency and eigenvalue of each outcome. However, if the operator is not diagonal in the computational basis (which is relatively common) one has to diagonalize it.

Consider an operator $\hat{O}$ which is not diagonal in the computational basis. We can transform it into a diagonal operator D by doing the following operation,

$$D = U\hat{O}U^\dagger \tag{35}$$

where U is a unitary matrix and $U^\dagger$ its complex transpose, $U^\dagger U = UU^\dagger = I$. Then, if we want to compute the expected value $\langle O\rangle$ given a general state $|\psi\rangle$, we have to measure $|\tilde{\psi}\rangle$ in the computational basis,

$$\langle O\rangle = \langle\psi|\,\hat{O}\,|\psi\rangle = \langle\psi|\,U^\dagger U\hat{O}U^\dagger U\,|\psi\rangle = \langle\tilde{\psi}|\,D\,|\tilde{\psi}\rangle \tag{36}$$

with $|\tilde{\psi}\rangle = U\,|\psi\rangle$. Notice that having applied the unitary U to the general state, the operator $\hat{O}$ is then diagonal in the computational basis.

The first operator that we measure is the Hamiltonian in eq.(32). Again, with a quantum computer, we can only perform two-qubit interactions, so we have to measure all the interactions between pairs of qubits separately. However, we can perform simultaneous measurements of commuting gates. The two-qubit Coulombian interaction h_C is diagonal in the computational basis:

$$h_C = \begin{pmatrix} 0 & 0 & 0 & 0 \\ 0 & 0 & 0 & 0 \\ 0 & 0 & 0 & 0 \\ 0 & 0 & 0 & U \end{pmatrix}$$

Then, the Coulombian energy per pair of particles is direct:

$$e_C = U \cdot P_{11} \tag{37}$$

where P_{11} is the probability of having the two qubits occupied. To get the total interaction energy for each state, one has to sum over all the pairs that suffer this interaction. Conveniently, they commute with each other so with a single wave function collapse one can have the total interacting energy of the outcome.

The hopping term is a bit trickier. First, we have to bring the target qubits together, and we do it as in the Trotter steps. The hopping interactions that are applied simultaneously in the Trotter steps commute, which means that once they are brought together we can also measure their hopping energy at once. However, different gates involving the same site do not commute so we can not measure the total hopping energy of the state at once. We optimize this procedure by splitting the measurement into 2 groups of self-commuting terms, odd-even sites and even-odd sites. The two-qubit operator to measure is:

$$h_h = -J \begin{pmatrix} 0 & 0 & 0 & 0 \\ 0 & 0 & e^{-i\phi} & 0 \\ 0 & e^{i\phi} & 0 & 0 \\ 0 & 0 & 0 & 0 \end{pmatrix} \tag{38}$$

which is non-diagonal, so we use the matrix U_h to diagonalize it.

$$U_h = -J \begin{pmatrix} 1 & 0 & 0 & 0 \\ 0 & \frac{\exp(i\phi/2)}{\sqrt{2}} & \frac{\exp(-i\phi/2)}{\sqrt{2}} & 0 \\ 0 & \frac{-\exp(i\phi/2)}{\sqrt{2}} & \frac{\exp(-i\phi/2)}{\sqrt{2}} & 0 \\ 0 & 0 & 0 & 1 \end{pmatrix} \tag{39}$$

The total energy per interaction is,

$$e_h = -J(P_{01} - P_{10}) \tag{40}$$

where the subindices of P stand for the occupation of the corresponding qubits. Finally, once we have the total interacting and hopping energies we have to repeat this process several times to collect statistics of the total energy of the system. For our work, we repeated the process $n = 1000$ times. Then we average the 1000 energies obtained and the result is the expected value of the energy.

The other operator that we measure in the 1×8 circuit is the current,

$$\hat{I} = \frac{i2\pi J}{L} \sum_{i,\sigma}^{L} \left(e^{i\phi} \hat{c}^{\dagger}_{i+1\sigma} \hat{c}_{i\sigma} - e^{-i\phi} \hat{c}^{\dagger}_{i\sigma} \hat{c}_{i+1\sigma} \right) \tag{41}$$

Notice that this operator is formally similar to the hopping term: it also involves non-adjacent qubits and not all the two-qubit operations commute. So as we did with the hopping energy, we have to put target qubits together and divide the operator measurement in different runs. Moreover, the associated two-qubit operator is also non-diagonal:

$$\hat{i} = \frac{i2\pi J}{L} \begin{pmatrix} 0 & 0 & 0 & 0 \\ 0 & 0 & -ie^{-\phi} & 0 \\ 0 & ie^{\phi} & 0 & 0 \\ 0 & 0 & 0 & 0 \end{pmatrix} \tag{42}$$

so we have to diagonalize it with the U_i matrix.

$$U_i = \begin{pmatrix} 1 & 0 & 0 & 0 \\ 0 & \frac{-\exp(i\phi/2)}{\sqrt{2}} & \frac{-i\exp(-i\phi/2)}{\sqrt{2}} & 0 \\ 0 & \frac{i\exp(i\phi/2)}{\sqrt{2}} & \frac{\exp(-i\phi/2)}{\sqrt{2}} & 0 \\ 0 & 0 & 0 & 1 \end{pmatrix} \tag{43}$$

The current of each two-qubit interaction is then:

$$j = \frac{i2\pi J}{L}(P_{01} - P_{10}) \tag{44}$$

After adding the current of all the corresponding two-qubit matrices, one gets the total current. Again, we repeat this process $n = 1000$ times and average the results to find the expected value of the current operator.

4 Results

4.1 Ground state energy

To apply an electric field to an interacting Fermi-Hubbard ground state, we first have to prepare it. In the adiabatic algorithm, δt and T are two independent parameters, each one related to a source of error. δt is related to the Trotterization whereas T is related to the adiabatic approximation. The values that they must take to achieve an optimal interacting ground state are not known a priori. However, from a quantum computing perspective, it is interesting to know the minimal number of Trotter steps that we need to prepare successfully the interacting ground state. The number of Trotter steps is:

$$N = \frac{T}{\delta t} \tag{45}$$

We find the minimum depth that our circuit requires to prepare a good ground state assessing the error of the latter by sweeping for different periods and number of Trotter steps, as shown in Figure 6. Each combination of the period and the number of Trotter steps fixes a discretization, eq.(45).

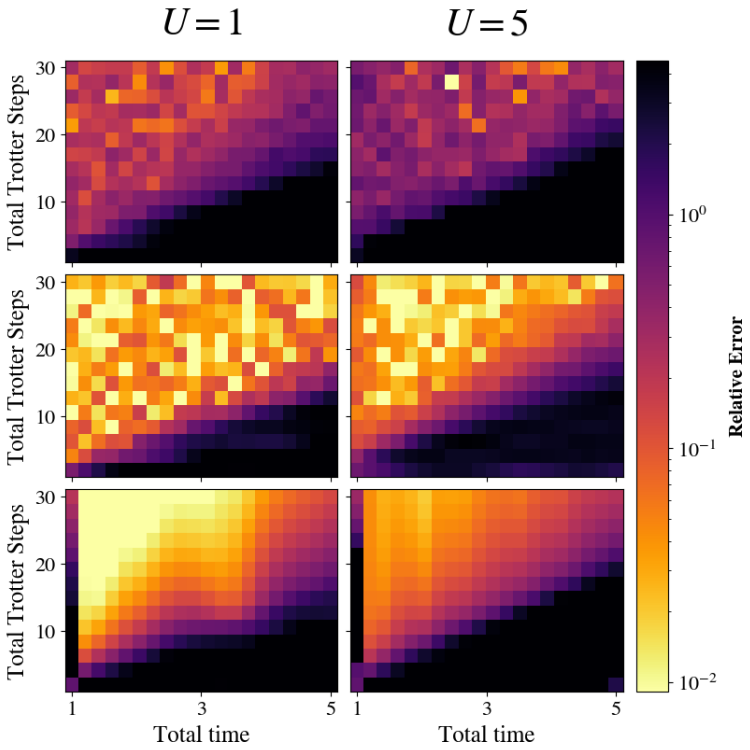

Figure 6: Density plots of the relative error in terms of the period of the adiabatic evolution T and the number of Trotter steps N. The left column shows the preparation of a weak interacting ground state ($U = 1$). The right column shows the preparation of a strong interacting ground state ($U = 5$). The system of the first two rows is the 1×8 ring with $n_\uparrow = 1$, $n_\downarrow = 1$ and $n_\uparrow = 3$, $n_\downarrow = 3$, from up to downwards. Their results have been measured with $n = 1000$ shots. The system of the third row is the 4×2 stacked ring with $n_\uparrow = 1$, $n_\downarrow = 1$ and we have measured the simulated wavefunction.

The relative error in the color bar of the plot is

$$\varepsilon = \frac{|E_f - E_{target}|}{|E_{target} - E_0|} \tag{46}$$

where E_f is the energy of our prepared state, E_0 is the non-interacting ground energy and E_{target} is the exact energy of the interacting ground state. Note that as δt and T are independent we could also do the density plot with the discretization δt instead of T.

The plot reveals that to prepare strongly interacting ground states we need more Trotter steps, which we could expect as the overlap between the target state and the $U = 0$ state is smaller. Additionally, the 1×8 quarter-filled ring needs the most Trotter steps to achieve a final state with an acceptable error, regardless of the period. The case where fewer Trotter steps are needed is the stacked ring, where for periods around $T = 2$ less than 20 Trotter steps are required to prepare a good state. All the states have been prepared in the absence of magnetic flux ($\phi = 0$). With the data of this plot, we fix the parameters of the state

preparation of each system, which are the same for both interactions.

$$1{\times}8 \text{ ring } (n_\uparrow = 1, n_\downarrow = 1) \quad \longrightarrow \quad N = 30,\ T = 3.8 \tag{47}$$

$$1{\times}8 \text{ ring } (n_\uparrow = 3, n_\downarrow = 3) \quad \longrightarrow \quad N = 26,\ T = 2.0 \tag{48}$$

$$4{\times}2 \text{ stacked ring } (n_\uparrow = 1, n_\downarrow = 1) \quad \longrightarrow \quad N = 26,\ T = 2.2 \tag{49}$$

4.2 Non-equilibrium

4.2.1 Uniform electric field

We now apply two electric fields to the previously prepared ground state with values $E_w = 0.05$ and $E_s = 0.25$. The response of each system is represented in Figure 7.

Period of the oscillations

The first thing we notice is that in all non-interacting cases (the green curves), the period $\tau = \frac{L}{E_0}$ is observed, regardless of the geometry (remind that we have taken $a = 1/L$ and $\Phi_0 = 1$). This period was derived analytically in [Zhe22] for single rings, and we also observed it in a double ring.

Also, we see that for the 1×8 ring and $n_\uparrow = 1$, $n_\downarrow = 1$ filling, the growing interaction does not remarkably affect the period of the current. However, for the two other systems, the currents in the interacting cases show an irregular oscillatory behaviour. The shapes of the curves follow a sinusoidal shape up to a specific time beyond which a damped oscillation pattern appears. This behaviour suggests that the wave function of these scenarios picks up contributions from eigenstates other than the equilibrium ground state.

Amplitude of the oscillations

Another interesting result is that the amplitude of the current does not depend on the electric field but on the filling. The curves with $n_\uparrow = 1$, $n_\downarrow = 1$ filling in different geometries show the same amplitude, which doesn't vary with the electric field. The $n_\uparrow = 3$, $n_\downarrow = 3$ filling shows higher current amplitude and is also independent of the field.

Electric field excitations

The fact that the period is inversely proportional to the electric field but the amplitude is invariant could lead us to the conclusion that the response current is only governed by the absolute value of the flux, and not by its variation. Prove of it is that the plots in the left row fit in the first 10 units of time of the plots in their right. However, there is one exception, the $U = 5$ red curve for the 1×8 ring in the 4th row (1×8, $n_\uparrow = 3$, $n_\downarrow = 3$) changes its behaviour with the growing electric field: it does not intersect the blue curve when the flux applied to the system is the same. This phenomenon indicates that due to the electric field intensity, the curve has gained a contribution of another equilibrium eigenstate, probably a more energetic one. In the other states with damped oscillations, we do not see this transition because the critical electric field is not in our range of study. However, we know that at arbitrary small electric field, we have to recover the equilibrium case where the current is driven by a single eigenstate, so there must exist a critical electric field for each system in which the instantaneous state excites and starts getting a contribution from other eigenstates. To gain confidence in this affirmation we perform a quench.

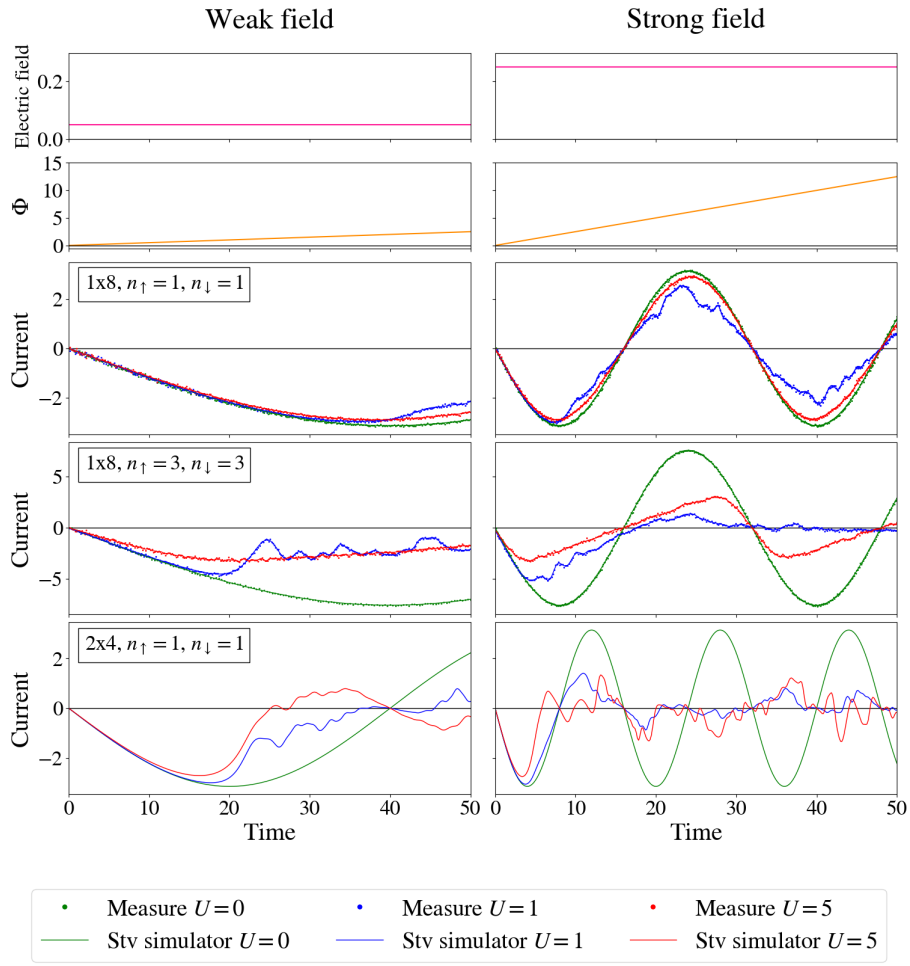

Figure 7: Response of the Fermi-Hubbard model to an electric field. The top row shows the electric field intensity. The second row shows the corresponding evolution of the magnetic flux over time. The next rows show the current response to the above electric field. The system and the filling studied in each row are labelled inside the plots. Measurements performed with $n = 1000$ shots.

4.2.2 Quench

The response of the current to a sudden turn-off of the electric field is represented in Figure 8. The first thing that catches our attention are the oscillations that appear in some cases after turning off the field. Notably, they only appear in the conditions where we find excited states in Figure 7. Although their existence could seem odd, the expected value of the current doesn't have to remain constant in a time-independent Hamiltonian since $[H, \hat{I}] \neq 0$. The other requirement to observe them is that the instantaneous state of each system is not an eigenvector of the Hamiltonian, but a linear combination of at least two, and we have already mentioned that the excited states of the last plot fulfil this requirement.

We are going to briefly develop the simplest state of an excited state to better understand why the quench oscillations appear. Consider the time evolution of the state $|\psi(t)\rangle$ in terms of two eigenvectors of the Hamiltonian with energies E_0 and E_1,

$$|\psi(t)\rangle = c_0 e^{-iE_0 t}|0\rangle + c_1 e^{-iE_1 t}|1\rangle = c_0 e^{i\Delta E t/2}|0\rangle + c_1 e^{-i\Delta E t/2}|1\rangle\,, \qquad c_0, c_1 \in \mathbb{C} \quad (50)$$

where $\Delta E = E_1 - E_0$. The expected value of the current for this state

$$\langle \hat{I} \rangle = \langle \psi(t) | \hat{I} | \psi(t) \rangle = |c_0|^2 \langle I_0 \rangle + |c_1|^2 \langle I_1 \rangle + 2\Re \left(co^* c_1 e^{-i\Delta E t} \langle 0 | \hat{I} | 1 \rangle \right) \tag{51}$$

clearly reflects a periodic behaviour dependent on the gap between the two eigenvalues with $\omega = \Delta E = \frac{2\pi}{T}$. Also, we see that the amplitude of the oscillations depends on the coefficient of each eigenstate.

With this result and the plot, we realize that the frequency of the oscillations gives an insight into the energy gaps involved in the excited states. Moreover, the growing amplitude of the oscillations with the electric field shows that the contribution of each eigenvector changes with the electric field, where probably the more energetic states are the ones that gain relevance. This phenomenon could not be inferred from Figure 7.

Finally, we can also observe the transition in the 1×8, $n_\uparrow = 3$, $n_\downarrow = 3$ $U = 5$ curve where for a weak field there are no appreciable oscillations and in the strong field case they become significant.

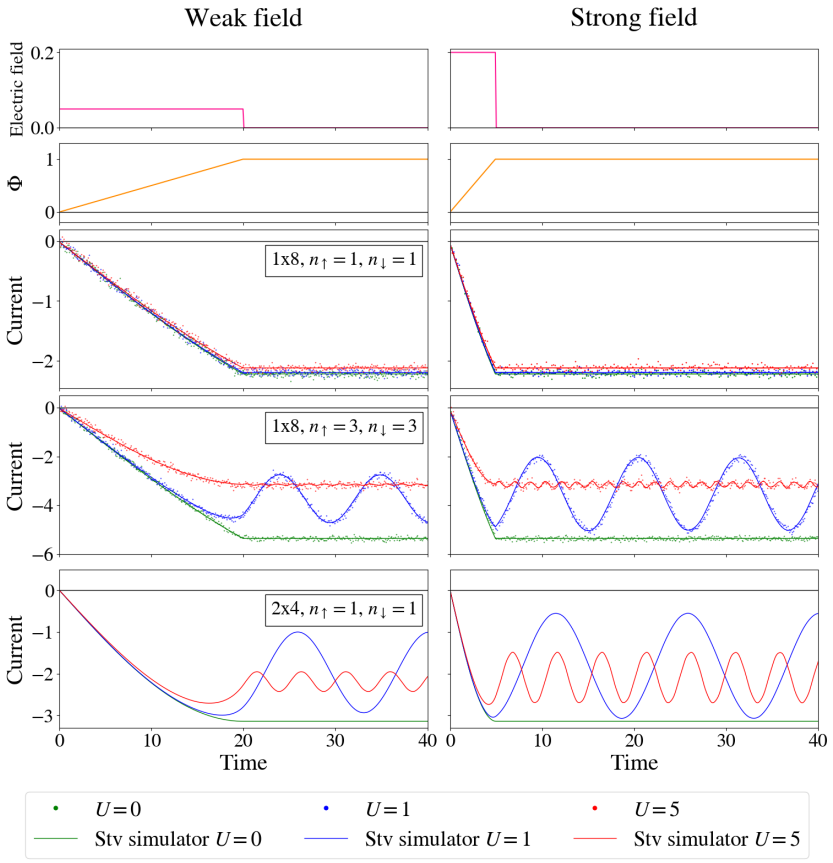

Figure 8: Response of the Fermi-Hubbard model to a quench of the electric field. The top row shows the electric field intensity. The second row shows the corresponding evolution of the magnetic flux over time. The next rows show the current response to the above electric field. The system and the filling studied in each row are labelled inside the plots. Measurements performed with $n = 1000$ shots.

5 Discussion

In this work, we have successfully simulated the response of the Fermi-Hubbard model to a uniform electric field for different interaction strengths, fillings and geometries, from a digital quantum approach. Concretely we have worked with a 1×8 ring with $n_\uparrow = 1$, $n_\downarrow = 1$ and $n_\uparrow = 3$, $n_\downarrow = 3$ filling and with a 4×2 stacked ring with $n_\uparrow = 1$, $n_\downarrow = 1$ filling. We started designing an adiabatic quantum algorithm based on Trotter steps to prepare interacting time-independent ground states for each system. For the 1×8 case, we have created a circuit with 59 gates and 11.5 layers of depth per Trotter step. For a general number of qubits N, both magnitudes scale linearly $O(N)$. Additionally, all the physical magnitudes that we wanted to observe from the 1×8 ring were obtained with a quantum measurement algorithm. For the 4×2 stacked ring, the circuit has 88 gates and 22 layers of depth per Trotter step. In this case, the number of gates scaling is polynomial with the number of qubits $O(N^2)$ and the depth scaling is linear $O(N)$. We assumed linear connectivity and local interactions between qubits in both cases.

Afterwards, we applied different electric fields to the prepared ground states using the same Trotter steps structure of the circuits. Our results show that the non-interacting systems match the period predicted by [Zhe22], which is the same period that the parabolas of the spectrum of time-independent flux Hamiltonian have. However, when the electrons are correlated, the smooth behaviour of the current breaks due to contributions from different eigenstates. Their irregular oscillatory pattern suggests that the instantaneous wave functions are not an eigenstate of the time-independent flux Hamiltonian. However, for arbitrarily small electric fields, one has to recover the equilibrium adiabatic limit where the instantaneous wave function is an eigenstate of the Hamiltonian, so for each system, there must exist a critical electric field below which the excited state is no longer excited. Related to this, we believe that we have observed this transition for the 1×8 $n_\uparrow = 3$, $n_\downarrow = 3$, $U = 5$ case.

To further study the nature of the instantaneous wave functions, we have performed a quench at time $t = \frac{\Phi_0}{E}$. After turning off the field we observe an oscillatory pattern in the excited states that was previously found by [M10]. The frequency of these oscillations gives us an insight into the energy gap between the components of the excited states, while their amplitude is related to the intensity of the electric field. Finding these properties of instantaneous states without resorting to the spectrum is relevant since accessing the time-dependent Hamiltonian can be very challenging for a growing number of sites.

This project opens the possibility of further work. First of all, preparing a fermionic ground state with a fixed number of particles and spins is non-trivial. In this work we did an initial approach by adding a chemical potential and a spin coupling term, however, we did not have unlimited freedom to costume the filling of our system. Adding a $\Phi \neq 0$ flux to the non-interacting Hamiltonian can give access to even-even combinations and adding adiabatically periodic boundary conditions can give access to even-odd or odd-even fillings, so we would like to follow this path to improve the ground state preparation of fermionic systems. Secondly, more systems with different numbers of sites and filling have to be studied to have a more general overview of the critical field and the maximum amplitude of the current, as well as running the simulations for longer times.

To our knowledge, there is not much literature on the effects of the electric field on the Hubbard model, nor on studying the dynamics in a digital quantum computing platform. In this sense, we hope that this work can provide an overview of how Hubbard rings respond to electric fields as well as how to cope with time-dependent Hamiltonians in quantum computing.

Bibliography

[AB59] Y. Aharonov and D. Bohm. Significance of electromagnetic potentials in the quantum theory. *Physical Review*, 115, 1959.

[BF28] M. Born and V. Fock. Beweis des adiabatensatzes. *Zeitschrift für Physik*, 51, 1928.

[CCBP+22] Mirko Consiglio, Wayne J. Chetcuti, Carlos Bravo-Prieto, Sergi Ramos-Calderer, Anna Minguzzi, José I. Latorre, Luigi Amico, and Tony J.G. Apollaro. Variational quantum eigensolver for su(n) fermions. *Journal of Physics A: Mathematical and Theoretical*, 55, 2022.

[CHKA22] Wayne J. Chetcuti, Tobias Haug, Leong Chuan Kwek, and Luigi Amico. Persistent current of su(n) fermions. *SciPost Physics*, 12, 2022.

[CRG89] Ho Fai Cheung, Eberhard K. Riedel, and Yuval Gefen. Persistent currents in mesoscopic rings and cylinders. *Physical Review Letters*, 62, 1989.

[DBK+22] Andrew J. Daley, Immanuel Bloch, Christian Kokail, Stuart Flannigan, Natalie Pearson, Matthias Troyer, and Peter Zoller. Practical quantum advantage in quantum simulation. *Nature*, 607, 2022.

[DXP+10] Jiangfeng Du, Nanyang Xu, Xinhua Peng, Pengfei Wang, Sanfeng Wu, and Dawei Lu. Nmr implementation of a molecular hydrogen quantum simulation with adiabatic state preparation. *Physical Review Letters*, 104, 2010.

[ERCBP+22] Stavros Efthymiou, Sergi Ramos-Calderer, Carlos Bravo-Prieto, Adrián Pérez-Salinas, Diego García-Martín, Artur Garcia-Saez, José Ignacio Latorre, and Stefano Carrazza. Qibo: a framework for quantum simulation with hardware acceleration. *Quantum Science and Technology*, 7, 2022.

[ES98] Konstantin Efetov and Ben Simons. Supersymmetry in disorder and chaos. *Physics Today*, 51, 1998.

[EW11] Martin Eckstein and Philipp Werner. Damping of bloch oscillations in the hubbard model. *Physical Review Letters*, 107, 2011.

[fho63] Electron correlations in narrow energy bands. *Proceedings of the Royal Society of London. Series A. Mathematical and Physical Sciences*, 276, 1963.

[GAN14] I. M. Georgescu, S. Ashhab, and Franco Nori. Quantum simulation. *Rev. Mod. Phys.*, 86:153–185, Mar 2014.

[JSK+18] Zhang Jiang, Kevin J. Sung, Kostyantyn Kechedzhi, Vadim N. Smelyanskiy, and Sergio Boixo. Quantum algorithms to simulate many-body physics of correlated fermions. *Physical Review Applied*, 9, 2018.

[Kat50] Tosio Kato. On the adiabatic theorem of quantum mechanics. *Journal of the Physical Society of Japan*, 5, 1950.

[LW68] Elliott H. Lieb and F. Y. Wu. Absence of mott transition in an exact solution of the short-range, one-band model in one dimension. *Physical Review Letters*, 20, 1968.

[MCK04] Santanu K. Maiti, J. Chowdhury, and S. N. Karmakar. Strange behavior of persistent currents in small hubbard rings. *Physics Letters, Section A: General, Atomic and Solid State Physics*, 332, 2004.

[MLA+22] Lars S. Madsen, Fabian Laudenbach, Mohsen Falamarzi Askarani, Fabien Rortais, Trevor Vincent, Jacob F.F. Bulmer, Filippo M. Miatto, Leonhard Neuhaus, Lukas G. Helt, Matthew J. Collins, Adriana E. Lita, Thomas Gerrits, Sae Woo Nam, Varun D. Vaidya, Matteo Menotti, Ish Dhand, Zachary Vernon, Nicolás Quesada, and Jonathan Lavoie. Quantum computational advantage with a programmable photonic processor. *Nature*, 606, 2022.

[M10] M. Mierzejewski, J. Łuczka, and J. Dajka. Current in hubbard rings manipulated via magnetic flux. *Journal of Physics Condensed Matter*, 22, 2010.

[POPSSR+22] Axel Pérez-Obiol, Adrián Pérez-Salinas, Sergio Sánchez-Ramírez, Bruna G.M. Araújo, and Artur Garcia-Saez. Adiabatic quantum algorithm for artificial graphene. *Physical Review A*, 106, 2022.

[PORM+23] A. Pérez-Obiol, A. M. Romero, J. Menéndez, A. Rios, A. García-Sáez, and B. Juliá-Díaz. Nuclear shell-model simulation in digital quantum computers, 2023.

[SBG+22] Stasja Stanisic, Jan Lukas Bosse, Filippo Maria Gambetta, Raul A. Santos, Wojciech Mruczkiewicz, Thomas E. O'Brien, Eric Ostby, and Ashley Montanaro. Observing ground-state properties of the fermi-hubbard model using a scalable algorithm on a quantum computer. *Nature Communications*, 13, 2022.

[SM16] Madhumita Saha and Santanu K. Maiti. Circulating current in 1d hubbard rings with long-range hopping: Comparison between exact diagonalization method and mean-field approach. *Physica E: Low-Dimensional Systems and Nanostructures*, 84, 2016.

[Zhe21] Yong Zheng. Exact solution of u→ 1d hubbard model in electric field. *Physics Letters, Section A: General, Atomic and Solid State Physics*, 394, 2021.

[Zhe22] Yong Zheng. Oscillating charge currents of one-dimensional hubbard model in electric field. *Journal of Physics: Conference Series*, 2313(1):012019, jul 2022.

A Derivation of the Fermi-Hubbard model

This derivation can be found in [CHKA22]. We are going to start with an electronic Hamiltonian in a static ionic lattice, which we can assume since the ions are much heavier than the electrons.

$$H = \sum_{i=1}^{N} \underbrace{\left(\frac{\mathbf{p}_i^2}{2m} + V(\mathbf{r}_i) \right)}_{h_1} + \sum_{1 \leq i \leq j \leq N} U(\mathbf{r}_i, \mathbf{r}_j) \tag{52}$$

where $V(\mathbf{r}_i)$ is a one-particle periodic potential and $U(\mathbf{r}_i, \mathbf{r}_j)$ is a two-particle effective potential and N is the number of particles. Since $V(\mathbf{r})$ is periodic, the eigenvectors of h_1 are Bloch functions of the form

$$\varphi_{\alpha\mathbf{k}}(\mathbf{r}) = e^{i\mathbf{k}\cdot\mathbf{r}} u_{\alpha\mathbf{k}}(\mathbf{r}) \tag{53}$$

where α is the band index, $\mathbf{k}$ is the quasi momentum and $u_{\alpha\mathbf{k}}(\mathbf{r})$ has the periodicity of the lattice. An equivalent one-particle basis is formed by the Wannier functions, which are centered on the lattice vectors $\mathbf{R}_i$. We can write them in terms of the Bloch functions Fourier transforming

$$w_{\alpha i}(\mathbf{r} - \mathbf{R}_i) = \frac{1}{\sqrt{L}} \sum_k e^{-i\mathbf{k}\cdot\mathbf{R}_i} \varphi_{\alpha\mathbf{k}}(\mathbf{r}) \tag{54}$$

where L is the number of sites. Then, we can define the field operator that creates an electron of spin σ at position $\mathbf{r}$ as:

$$\hat{\Psi}_\sigma^\dagger(\mathbf{r}) = \sum_{\alpha,i} w_{\alpha i}^*(\mathbf{r} - \mathbf{R}_i) \hat{c}_{\alpha i,\sigma}^\dagger \tag{55}$$

where $\hat{c}_{\alpha i,\sigma}^\dagger$ is the creation operator of an electron of spin σ in the Wannier state $w_{\alpha i}(\mathbf{r} - \mathbf{R}_i)$. Knowing this, we can rewrite the Hamiltonian in eq.(52),

$$H = \sum_\sigma \int d\mathbf{r}\ \hat{\Psi}_\sigma^\dagger(\mathbf{r}) h1 \hat{\Psi}_\sigma(\mathbf{r}) + \sum_{\sigma,\varsigma} \int d\mathbf{r}_i d\mathbf{r}_j\ \hat{\Psi}_\sigma^\dagger(\mathbf{r}_i) \hat{\Psi}_\varsigma^\dagger(\mathbf{r}_j) U(\mathbf{r}_i, \mathbf{r}_j) \hat{\Psi}_\varsigma(\mathbf{r}_j) \hat{\Psi}_\sigma(\mathbf{r}_i) \tag{56}$$

and then second quantizing it reads:

$$H = \sum_{\alpha,i,j,\sigma} J_{ij}^\alpha \hat{c}_{\alpha i,\sigma}^\dagger \hat{c}_{\alpha j,\sigma} + \sum_{\substack{\alpha,\beta,\gamma,\delta \\ i,j,k,l}} \sum_{\sigma,\varsigma} U_{i,j,k,l}^{\alpha,\beta,\gamma,\delta} \hat{c}_{\alpha i,\sigma}^\dagger \hat{c}_{\beta j,\varsigma}^\dagger \hat{c}_{\gamma k,\varsigma} \hat{c}_{\delta l,\sigma} \tag{57}$$

The hopping and interaction matrix elements of the previous equation are respectively:

$$J_{ij}^\alpha = \int d\mathbf{r}\ w_{\alpha i}^*(\mathbf{r} - \mathbf{R}_i) h_1 w_{\alpha j}(\mathbf{r} - \mathbf{R}_j) \tag{58}$$

$$U_{i,j,k,l}^{\alpha,\beta,\gamma,\delta} = \int d\mathbf{r}_1 d\mathbf{r}_2\ w_{\alpha i}^*(\mathbf{r} - \mathbf{R}_i) w_{\beta j}^*(\mathbf{r} - \mathbf{R}_j) U(\mathbf{r}_1, \mathbf{r}_2) w_{\gamma k}(\mathbf{r} - \mathbf{R}_k) w_{\delta l}(\mathbf{r} - \mathbf{R}_l) \tag{59}$$

We are interested in the lowest energies of the Hamiltonian and if we assume that all bands except the first one are far away from the Fermi-level, we can transform our Hamiltonian into a one-band model. Additionally, we apply the tight-binding approximation in which only the nearest neighbour hopping interactions are relevant, we assume that the intra-atomic Coulomb interaction is much larger than the inter-atomic, and translational invariance. We end up with:

$$H = -J \sum_{\langle i,j \rangle,\sigma} \left(\hat{c}_{i\sigma}^\dagger \hat{c}_{j\sigma} + \hat{c}_{j\sigma}^\dagger \hat{c}_{i\sigma} \right) + U \sum_i \hat{n}_{i\uparrow} \hat{n}_{i\downarrow} \tag{60}$$

which is exactly eq.(1).

B Analytical solution of the 1D Hamiltonian

The solutions developed below are not the only possible analytical solutions of the Hamiltonian but they are two simple examples of how to treat the Fermi-Hubbard model. We consider the 1D Fermi-Hubbard model without electromagnetic coupling

$$\hat{H}_0 = \underbrace{-J\sum_{i,\sigma}\left(\hat{c}^\dagger_{i+1\sigma}\hat{c}_{i\sigma} + \hat{c}^\dagger_{i\sigma}\hat{c}_{i+1\sigma}\right)}_{H_{hopp}} + \underbrace{U\sum_{i}^{L}\hat{n}_{i\uparrow}\hat{n}_{i\downarrow}}_{H_C} \tag{61}$$

B.1 Solution of H_{hopp}, $U = 0$

As we have seen in the previous section, H_{hopp} comes from a monoparticular Hamiltonian in first quantization with a kinetic term and a periodic potential, under the tight-binding approximation. This kind of Hamiltonians are diagonal in the quasi-momentum basis, so if we want to solve H_{hopp} we have to Fourier transform the fermionic operators in eq.(61),

$$\hat{a}^\dagger_{q\sigma} = \frac{1}{\sqrt{L}}\sum_j e^{iq\cdot j}\hat{c}^\dagger_{j\sigma} \tag{62}$$

$$\hat{a}_{q\sigma} = \frac{1}{\sqrt{L}}\sum_j e^{-iq\cdot j}\hat{c}_{j\sigma} \tag{63}$$

where $\hat{a}^\dagger_{q\sigma}$ and $\hat{a}_{q\sigma}$ create and destroy a particle of quasi-momentum q and spin σ, respectively. Because of the periodic boundary conditions, the quasi-momentum q is quantized and is

$$q = \frac{2\pi j'}{L}, \qquad j' \in [0, 1, 2, ..., L-1] \tag{64}$$

To plug the momentum operators into the Hamiltonian it is more comfortable to write the inverse of eq.(62, 63)

$$\hat{c}^\dagger_{j\sigma} = \frac{1}{\sqrt{L}}\sum_{j'} e^{-i\frac{2\pi j'}{L}\cdot j}\hat{a}^\dagger_{q\sigma} \tag{65}$$

$$\hat{c}_{j\sigma} = \frac{1}{\sqrt{L}}\sum_{j'} e^{i\frac{2\pi j'}{L}\cdot j}\hat{a}_{q\sigma} \tag{66}$$

With this modification, the 1D non-interacting Hamiltonian reads:

$$\hat{H}_0 = -\frac{J}{L}\sum_{j,\sigma}\left(\sum_{j',\sigma} e^{-i\frac{2\pi j'}{L}\cdot(j+1)}\hat{a}^\dagger_{q\sigma}\sum_{i',\sigma} e^{i\frac{2\pi i'}{L}\cdot j}\hat{a}_{q'\sigma} + \sum_{i',\sigma} e^{-i\frac{2\pi i'}{L}\cdot j}\hat{a}^\dagger_{q'\sigma}\sum_{j',\sigma} e^{i\frac{2\pi j'}{L}\cdot(j+1)}\hat{a}_{q\sigma}\right) =$$

$$-\frac{J}{L}\sum_{j,\sigma}\left(\sum_{j',\sigma}\sum_{i',\sigma} e^{i\frac{2\pi j}{L}\cdot(i'-j')-i\frac{2\pi j'}{L}}\hat{a}^\dagger_{q\sigma}\hat{a}_{q'\sigma} + \sum_{i',\sigma}\sum_{j',\sigma} e^{i\frac{2\pi j}{L}\cdot(j'-i')+i\frac{2\pi j'}{L}}\hat{a}^\dagger_{q'\sigma}\hat{a}_{q\sigma}\right) =$$

$$-\frac{J}{L}\left(\sum_{j',\sigma}\sum_{i',\sigma}\underbrace{\sum_{j,\sigma} e^{i\frac{2\pi j}{L}\cdot(i'-j')}}_{\delta_{i'j'}\cdot L} - i\frac{2\pi j'}{L}\hat{a}^\dagger_{q\sigma}\hat{a}_{q'\sigma} + \sum_{i',\sigma}\sum_{j',\sigma}\underbrace{\sum_{j,\sigma} e^{i\frac{2\pi j}{L}\cdot(j'-i')}}_{\delta_{i'j'}\cdot L} + i\frac{2\pi j'}{L}\hat{a}^\dagger_{q'\sigma}\hat{a}_{q\sigma}\right) =$$

$$-J\left(\sum_{j',\sigma} e^{-i\frac{2\pi j'}{L}}\hat{a}^{\dagger}_{q\sigma}\hat{a}_{q\sigma} + \sum_{j',\sigma} e^{i\frac{2\pi j'}{L}}\hat{a}^{\dagger}_{q\sigma}\hat{a}_{q\sigma}\right) =$$

$$\hat{H}_0 = -J\sum_{j',\sigma} 2\cos\left(\frac{2\pi j'}{L}\right)\hat{a}^{\dagger}_{q\sigma}\hat{a}_{q\sigma} \tag{67}$$

As we can see, the non-interacting 1D Hamiltonian is diagonal in momentum basis. Then, its eigenfunctions are Bloch functions with quasi-momentum $q = \frac{2\pi j'}{L}$ and its eigenvalues are $E_{j'} = -2J\cos(q)$. The ground state corresponds to $j' = 0$ with $E_0 = -2J$

B.2 Solution of H_C, $J = 0$

In the $J = 0$ limit, we remove the hopping term from the Hamiltonian and it reads,

$$\hat{H}_0 = U\sum_{i}^{L} \hat{n}_{i\uparrow}\hat{n}_{i\downarrow} \tag{68}$$

As it is easy to see, this Hamiltonian is diagonal in the Fock (or Wannier) basis. The ground state is the one with $E = 0$. The energy spectrum is

$$E_n = nU \tag{69}$$

where n is the index of excitation which is equal to the number of double-occupied sites. If $n = 0$ we are in the ground state, and for $n = 1$ we are in the first excited state and so on. The spectrum is degenerate (since for most number of particles there are many combinations of occupations that do not have two electrons in the same site). If we do not fix the number of particles, the exact expression for the degeneracy is

$$deg = \binom{L}{n}\cdot 3^{L-n} \tag{70}$$

where n stands for the number of double-occupied sites. We can check that

$$\sum_{n=0}^{L}\binom{L}{n}\cdot 3^{L-n} = 4^L = dim\ \mathcal{H} \tag{71}$$

where $\mathcal{H}$ is the Hilbert space.

C Computing Peierls phase

In this Appendix we are going to compute the Peierls phase of a magnetic field and an electric field. The Peierls phase is:

$$\phi = \frac{e}{c\hbar}\int_i^j \mathbf{A}\cdot\mathbf{dl} \tag{72}$$

where $\mathbf{A}$ is the electromagnetic potential that fulfils:

$$-\frac{\partial\mathbf{A}}{\partial t} = \mathbf{E} \tag{73}$$

$$\nabla\times\mathbf{A} = \mathbf{B} \tag{74}$$

$$\oint_C \mathbf{E} \cdot \mathbf{dl} = -\int_S \frac{\partial \mathbf{B}}{\partial t} \cdot \mathbf{dS} \tag{75}$$

As the above equation reveals, to compute the Peierls phase we need to take into account the geometry of our system. We do the derivation for the 1D chain with periodic boundary conditions which is easily extended to the stacked ring case.

As we work with a ring, we use cylindrical coordinates $(\hat{r}, \hat{\theta}, \hat{z})$, and we assume that the ring is centered on the origin of coordinates and in the $x-y$ plane. Looking at eq.(3), the first thing we notice is that to avoid the vanishing of the Peierls phase, the electromagnetic potential has to be parallel to the line that connects two sites, ie. parallel to the $\hat{\theta}$ direction. Secondly, looking at eq.(73,74) we can see that the coupling of an electric field needs a time-dependent Hamiltonian, while the magnetic field does not. We start with the simpler time-independent case and then we will move on to the other.

C.0.1 Magnetic field

The electromagnetic potential must be in the $\hat{\theta}$ direction to be non-vanishing, such as:

$$\mathbf{A} = \left(0, \frac{rB_0}{2}, 0\right) \tag{76}$$

Following eq. (74), the associated magnetic field is

$$\mathbf{B} = (0, 0, B_0) \tag{77}$$

If we then compute the Peierls phase,

$$\phi_{\mathbf{B}} = \frac{e}{c\hbar} \int_{\mathbf{r}_i}^{\mathbf{r}_j} \mathbf{A} \cdot \mathbf{dl} \; = \frac{e}{c\hbar} \int_{\mathbf{r}_i}^{\mathbf{r}_j} \frac{RB_0}{2} \cdot r d\theta \; = \frac{2\pi\Phi}{cL\Phi_0} \tag{78}$$

where $\Phi_0 = \frac{h}{e}$ is the flux quantum, being R the radius of the chain and Φ is the magnetic flux that fulfils:

$$\Phi = \int_S \mathbf{B} \cdot \mathbf{dS} = B_0 \pi R^2 \tag{79}$$

C.0.2 Electric field

To couple an electric field, we must choose another $\mathbf{A}$. We want one that creates an electric field parallel to the ring:

$$\mathbf{A} = (0, E(r) \cdot t, 0) \tag{80}$$

$$E(r) = \frac{1}{2} r B_0 \tag{81}$$

This electromagnetic potential represents a uniform electric field at fixed r, following eq.(73). Moreover, following eq.(74) we see that also represents a linearly increasing magnetic field with magnitude B_0 in the $\hat{z}$ direction. Writing it down:

$$\mathbf{E} = (0, E_0, 0) \tag{82}$$

$$\mathbf{B} = (0, 0, B_0 \cdot t) \tag{83}$$

with $E_0 = -\frac{1}{2} R B_0$. In this case, the Peierls phase is:

$$\phi_{\mathbf{E}} = \frac{e}{c\hbar} \int_i^j \mathbf{A} \cdot \mathbf{dl} \; = \frac{e}{c\hbar} \int_i^j E(r) \cdot t \cdot r \, d\theta = \frac{e 2\pi R}{c\hbar L} E_0 \cdot t = \frac{2\pi a}{\Phi_0 c} E_0 \cdot t \tag{84}$$

we have defined the lattice parameter $a = \frac{2\pi R}{L}$. Note that we have used cylindrical coordinates because we have approximated our periodical chain with L number of sites to a circular ring. However, the result of the derivation is the same for any regular polygon centered at the origin using cartesian coordinates $(\hat{x}, \hat{y}, \hat{z})$.

D Aharonov-Bohm effect

We start considering a monoparticular Hamiltonian with only a kinetic term:

$$H = \frac{\mathbf{p}^2}{2m} \tag{85}$$

When applying a magnetic field $\mathbf{B}$ associated with a vector potential $\mathbf{A}(\mathbf{r})$, the momentum transforms, and so the Hamiltonian:

$$\mathbf{p} \longrightarrow \mathbf{p} - e\mathbf{A} \tag{86}$$

$$H = \frac{(\mathbf{p} - e\mathbf{A})^2}{2m} \tag{87}$$

We now place our particle at $\mathbf{r_0}$, where $\mathbf{A}$ vanishes (we can always do this because of Gauge freedom). We denote the ground state of the Hamiltonian in eq.(87) as $\Psi(\mathbf{r} - \mathbf{r_0})$. If we now move the particle in some path in space until $\mathbf{r_1}$, the electromagnetic potential experienced by the particle changes, ie. its momentum, and now the lowest eigenstate of the Hamiltonian has transformed to:

$$\Psi(\mathbf{r} - \mathbf{r_1}) = \exp\left(\frac{ie}{\hbar}\int_{\mathbf{r_0}}^{\mathbf{r_1}} \mathbf{A}(\mathbf{r}) \cdot d\mathbf{r}\right) \Psi(\mathbf{r} - \mathbf{r_0})$$

which is easy to check by substituting it in the time-independent Schrödinger equation. However, if we now move the particle in a loop C and bring it back to $\mathbf{r_0}$, the integral above reads:

$$\frac{ie}{\hbar}\oint_C \mathbf{A}(\mathbf{r}) \cdot d\mathbf{r} = \frac{ie}{\hbar}\oint_C \mathbf{A}(\mathbf{r}) \cdot r d\varphi = \frac{i2\pi\Phi}{\Phi_0}$$

so the wavefunction "picks up" a phase as it travels in a closed path, and it becomes a periodical function of the flux quantum Φ_0. Such a phenomenon is due to the Aharonov-Bohm effect [AB59], which proves that electromagnetic potential is not only a mathematical construct but a magnitude with physical implications. This effect is often observed in mesoscopic rings, since they are smaller than the electron's phase coherence length, that is, the typical distance the electron travels before it scatters inelastically. We must note that the existence of persistent current still holds in the presence of Coulombian interactions, as the flux dependence in the Hamiltonian is reflected in the kinetic one-body operator of the many-body Hamiltonian.